Langmuir

Article

pubs.acs.org/Langmuir

Strategies toward Enhanced Low-Pressure Volumetric Hydrogen Storage in Nanoporous Cryoadsorbents

Afsana Ahmed,[†,‡] Aaron W. Thornton,*[,‡] Kristina Konstas,[‡] Sridhar Kumar Kannam,[†] Ravichandar Babarao,[‡] B. D. Todd,[†] Anita J. Hill,[§] and Matthew R. Hill[‡]

[†]Mathematics Discipline, Faculty of Engineering and Industrial Science and Centre for Molecular Simulation, Swinburne University of Technology, Melbourne, Victoria 3122, Australia

[‡]Materials Science and Engineering and [§]Process Science and Engineering, CSIRO, Private Bag 33, Clayton South MDC, Victoria 3169, Australia

Supporting Information

ABSTRACT: The volumetric hydrogen capacity remains one of the most challenging criteria for on-board hydrogen storage system requirements. Here a new concept for hydrogen storage of porous aromatic frameworks (PAFs) impregnated with lithium-decorated fullerenes (Li_6C_{60}) is described. The loading of Li_6C_{60} and the effect on the adsorption of hydrogen (H_2) has been investigated by molecular simulation. It is shown that the incorporation of Li_6C_{60} can enhance the volumetric capacity of H_2 from 12 to 44 g L^{-1}, a 260% increase at 10 bar and 77 K. The impregnation of Li_6C_{60} increases the heat of adsorption and surface area at the cost of the available pore volume. However, the increase in adsorbed hydrogen outweighs any pore volume loss under optimized Li_6C_{60} loading and operating conditions. In addition, the H_2 volumetric uptake is shown to correlate with the volumetric surface area at all pressures whereas the H_2 gravimetric uptake correlates with the heat of adsorption at low pressures, surface area at moderate pressures, and pore volume at high pressures.

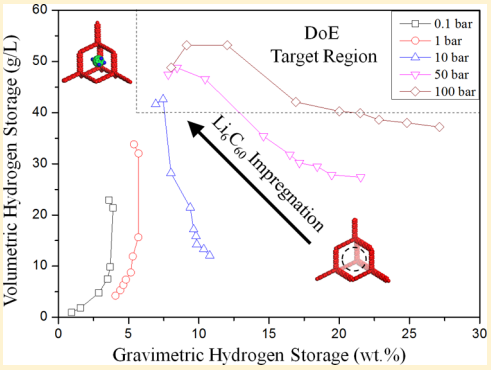

I. INTRODUCTION

During the past decade, a significant amount of research has been performed on nanoporous materials, which not only possess high surface areas but also reversibly adsorb or desorb hydrogen under pressure-swing and temperature-swing conditions.[1−9] They possess intrinsically high surface areas and internal volumes, and these factors are known to enhance gas storage at cryogenic temperatures.[10] A recent report from the U.S. Department of Energy (DoE) suggests that cryosorbents[11] are promising on-board hydrogen storage systems, although the capacity targets are yet to be met.[11] Even though cryoconditions are not within the DoE requirements, there is considerable research in cryocompressed systems to meet the DoE capacity targets.[12−16] Hydrogen has always been considered to be a medium for clean energy because of its universal abundance and lack of carbon emissions during use. The production of hydrogen remains a challenge, although technologies such as the steam reformation of coal/oil/gas,[17] fermentation of organic waste,[18] photodecomposition of water or organic compounds using bacteria,[19] and photocatalytic water splitting[20] are viable options. To make the hydrogen-driven fuel cell vehicle viable, efficient, safe, and economically sound hydrogen storage systems are needed.[21] A few years ago, the U.S. DoE set a number of targets for hydrogen storage systems including capacity requirements: 4.5 wt % or 28 g L^{-1} by the year 2010 and 5.5 wt % or 40 g L^{-1} by the year 2017.[11] Physical adsorbents have achieved high hydrogen capacities but usually at cryogenic temperatures. Fortunately, engineering work has pushed the viability of cryocompressed hydrogen into the realm of industrial feasibility.[11−16]

Designing adsorbent materials by tailoring the heat of adsorption, surface area, and pore volume is an effective strategy for enhancing the hydrogen capacity. Some of the leading candidates include metal−organic frameworks (MOFs)[22−27] and covalent organic frameworks (3D COFs)[28−32] with surface areas of up to 7000 m^2 g^{-1} (Farha et al.[33]) and 5172 m^2 g^{-1} (Babarao et al.[34]), respectively. The most important drawback of most of the MOFs and COFs is their low chemical stability. The development of porous aromatic framework (PAF) materials provides a combination of ultrahigh surface area and high physicochemical stability.

PAFs were recently reported as a new family of ultraporous materials with BET surface areas above 5000 m^2 g^{-1}.[35,36] Consisting of fused diamandoid tetrahedra with pore size distributions centered around 12 Å, these carbonaceous materials have been shown to deliver hydrogen storage capacities of 7 wt % at 48 bar and 77 K. These values, although when compared to most materials are exceptional, are

Received: October 7, 2013
Revised: November 26, 2013
Published: November 27, 2013

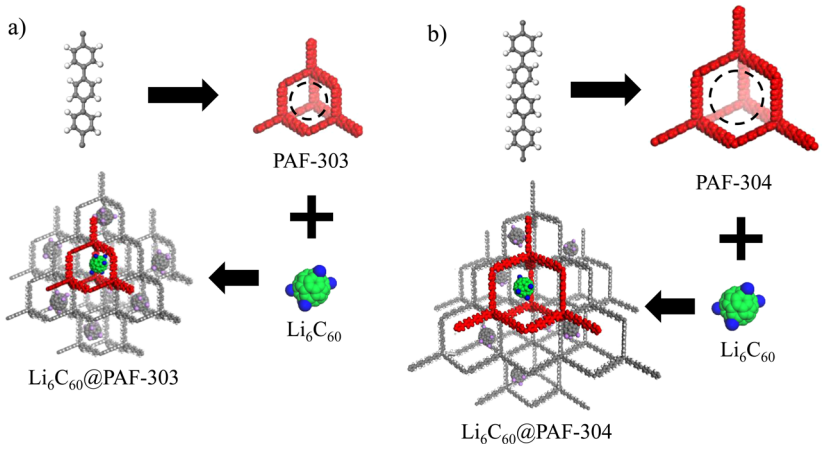

Figure 1. Atomistic representation of (a) PAF-303 and (b) PAF-304 impregnated with Li_6C_{60}. The PAF unit cell is highlighted in red, and Li_6C_{60} is highlighted in blue (lithium) and green (carbon).

lower than what might be expected given the large surface area and may be attributed to the inert, nonpolarized surface. However, PAFs are extremely stable and have been previously shown to be resistant to 7 days of immersion in boiling water.[35] This stability to harsh chemical environments facilitates the functionalization of the inert PAF surface with reactive, charged moieties to enhance the gas storage capacity. For example, we recently demonstrated that pyrophoric lithium species could be covalently bound to the PAF surface, tripling its CO_2 storage capacity without affecting the overall PAF architecture.[37]

Although PAFs can be tailored for excellent gravimetric storage capacity, less progress has been made in enhancing the volumetric performance, a key performance criterion for mobile applications. The 2017 DoE target is 40 g (useable H_2)/L (system). The best nanoporous adsorbents to date can barely meet these requirements, even under an idealized scenario where the adsorbent packing is assumed to be perfect, all adsorbed gas is useable, and the weight and size of the storage system are not accounted for.[38,39] Therefore, the next stage of development for improved hydrogen storage materials needs to focus upon strategies to enhance the volumetric storage capacity. Here, we detail the potential of one such approach, the impregnation of PAFs with lithiated fullerenes.

Previously we reported a concept to enhance both the gravimetric and volumetric gas storage capacity of MOFs drastically by infusing these porous media with metalated fullerenes.[40] This provided an additional surface within the same given volume, with metal sites polarizing hydrogen molecules. As a result, the enthalpy of adsorption was found to increase to 11 kJ mol^{-1} in concert with a drastically increased hydrogen storage capacity at low pressures. Metalated fullerenes are extremely reactive species and therefore require incorporation into particularly stable porous media for this concept to be realized. The stability of the porous media is imperative, and PAFs have the function and capability to facilitate the isolation of native or metalated fullerenes.

It is of interest in this study to determine the optimal amount of impregnation to maximize the volumetric uptake by utilizing molecular simulation techniques. Molecular simulation has proven to provide accurate predictions of hydrogen uptake in PAFs as shown by Lan et al.[41] The effect of impregnation on hydrogen uptake in MOFs has been successfully simulated by Rao et al.,[42] proving a useful route to increasing both gravimetric and volumetric uptake. Here we follow the same procedure to investigate lithiated fullerene impregnation within two PAFs with different pore sizes and explore the relationships between storage performance and structure characteristics described by Frost et al.[43]

II. MODELS AND SIMULATION

In this work, the PAF structures were constructed following details outlined by Lan et al.[41] The structures include PAF-30X (X = 3 to 4), where 3 indicates 3D structure and X denotes the number of phenyl rings used to replace the C−C bond. Each unit cell was constructed using the Forcite module of the Material Studio package with cubic periodic boundaries of dimensions ($a = b = c$) 33.80 and 43.55 Å for PAF-303 and PAF-304, respectively.[44] The pore windows for PAF-301 and PAF-302 were found to be too small for the impregnation of Li_6C_{60}. The diameters of the largest cavities of PAF-303 and PAF-304 were 20.8 and 28.6 Å, respectively. The atomistic representation of PAF-303 and PAF-304 impregnated with Li_6C_{60} is shown in Figure 1.

Six lithium ions were distributed over the five-membered rings of C_{60} at an approximate distance of 2.229 Å by geometry optimization,[45] forming Li_6C_{60}. Six lithium ions were chosen rather than 12 because it has been shown that Li_6C_{60} is the more stable compound.[46] The pore size distribution for the PAFs and lithiated fullerene-impregnated PAFs is shown in Figure S2 in the Supporting Information. A varying number n of lithiated fullerenes (nLi_6C_{60}) were randomly inserted in the PAF unit cell followed by geometry optimization. The prediction of hydrogen uptake inside the nLi_6C_{60}@PAF structures was calculated by the grand canonical Monte Carlo (GCMC) routine. In this method, the sorbate structure (H_2 gas) and the sorbent structure (nLi_6C_{60}@PAF) are treated as rigid. Trial addition, deletion, translation, and rotational moves of the H_2 gas molecule are repeated and accepted/rejected on the basis of the grand canonical ensemble at specific temperature and pressure. Two million equilibration steps are followed by 1 million production steps, ensuring that the final composition represents the state of thermodynamic equilibrium. The gravimetric capacity is expressed as wt % with the relation [(mass of H_2)/(mass of H_2 + mass of structure)], and the volumetric capacity is expressed in units of g L^{-1} with the relation [(mass of H_2)/(volume of unit cell)]. The interactions among H_2, PAF, and Li_6C_{60} were modeled by the Morse potential function given as

dx.doi.org/10.1021/la403864u | *Langmuir* 2013, 29, 15689−15697

$$U_{ij}(r_{ij}) = U_0(X^2 - 2X) \quad (1)$$

where

$$X = \exp\left[\frac{-\gamma}{2}\left(\frac{r_{ij}}{r_0} - 1\right)\right]$$

Here the parameter U_0 is the well depth, r_0 is the equilibrium bond distance, r_{ij} is the distance between atoms i and j, and γ is the force constant. We adopt the force field parameters that were calculated using first principles by Han and Goddard[2] for H_2-H_2 interactions, Lan et al.[41] for H_2–PAF interactions, and Rao et al.[42] for $H_2-Li_6C_{60}$ interactions, listed in Table 1.

Table 1. Force Field Parameters Employed in the Present Work[a]

atom types	U_0 (kcal mol^{-1})	r_0 (Å)	γ	ref
H_A–H_A	0.0182	3.570	10.709	Han and Goddard[2]
H_A–H_S	0.0124	3.201	12.003	Lan et al.[41]
H_A–C_R	0.0892	3.240	11.600	Lan et al.[41]
H_A–C_3	0.0620	3.240	11.006	Lan et al.[41]
H_A–Li	1.5970	1.994	7.940	Rao et al.[42]
H_A–C_C_{60}	0.1008	3.120	12.006	Rao et al.[42]

[a]Here, H_A denotes the hydrogen atom in the H_2 molecule, H_S denotes hydrogen in the PAF structure, and C_R denotes the resonantly coordinated carbon and C_3 denotes the tetrahedrally coordinated carbon in the PAF structure, Li denotes the lithium ion, and C_C_{60} denotes the carbon in the fullerene.

Although there is no high-pressure data to test the accuracy of the simulations, the force fields are derived from quantum calculations and therefore are applicable at any pressure.[47]

Molecular simulation results are given as the total hydrogen uptake including the gas-phase and adsorbed-phase contributions. Experimental results are usually reported as excess uptake, which is the total uptake minus the gas-phase contribution. Our simulated total uptake may be converted to excess uptake by predicting the gas-phase contribution using the Peng–Robinson equation of state and the pore volume of the PAF structures.

III. RESULTS AND DISCUSSION

First we evaluate the effect of impregnation at low pressures up to 1 bar in Figure 2 for PAF-303 and Figure 3 for PAF-304. The different trends between gravimetric and volumetric uptake with the Li_6C_{60} loading are highlighted with arrows to emphasize the results of this study. The significant difference is that the gravimetric uptake increasing trend reaches a maximum whereas the volumetric uptake continues to benefit at high Li_6C_{60} loading. This is a promising indication that volumetric uptake can be improved with impregnation.

The maximum gravimetric uptake of H_2 at 1 bar was found to be 5.71 wt % in PAF-304 impregnated with 28 Li_6C_{60}, which is approximately a 40% increase compared to that of bare PAF. The maximum H_2 uptake for PAF-303 was found to be 5.5 wt % with 9Li_6C_{60}, an 80% increase. Moreover, the maximum numbers of impregnated Li_6C_{60} that can fit within the PAF unit cells are 72 (or 91.73 wt %) for PAF-304 and 32 (or 87.41 wt %) for PAF-303, resulting in the lowest gravimetric uptake. There are two reasons for the maximum uptake at a particular loading. First, the highest gravimetric storage capacity is due to the highest N_2-accessible surface area (m^2/m^3), shown in Figure 8 and also mentioned in the supporting documents. Second, the mass of the material increases with loading whereas the volume of the material remains constant; therefore, the gravimetric uptake reaches a maximum where the benefit of uptake is overcome with the loss of material mass while the volumetric uptake continually increases.

Volumetric uptake results are given in Figure 2b for PAF-303 and Figure 3b for PAF-304 with various loadings of Li_6C_{60}. The maximum volumetric uptake of H_2 was 39.23 g L^{-1} in PAF-304 impregnated with 72 Li_6C_{60}. For PAF-303, the maximum volumetric H_2 uptake was 39.60 g L^{-1} with 32Li_6C_{60}. H_2 uptake increases with the loading of Li_6C_{60}, and in both cases, 40 g L^{-1} is almost achieved for the optimal Li_6C_{60} loading at just 1 bar pressure.

The next series of simulations is for higher pressures up to 100 bar, presented in Figure 4 for PAF-303 and Figure 5 for PAF-304. For gravimetric uptake, there is a critical pressure between 1 and 10 bar where there is no benefit to having impregnated Li_6C_{60} within the framework, as shown in Figures 4a and 5a. It is clear for gravimetric uptake that the incorporation of Li_6C_{60} inside the PAFs ensures a favorable environment for H_2 molecules at low pressure but has a detrimental effect at larger pressures. These results are attributed to the relative influence of the heat of adsorption, surface area, and pore volume at different pressures (vide infra).

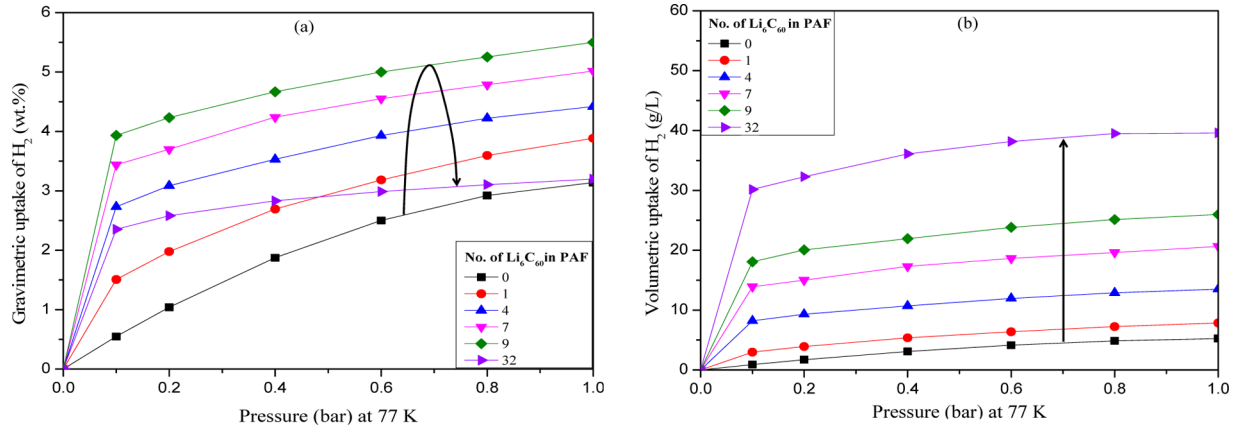

Figure 2. Total H_2 uptake in PAF-303: (a) gravimetric and (b) volumetric uptake embedded with the number of Li_6C_{60} molecules up to 1 bar and 77 K. Arrows indicate increased Li_6C_{60} loading.

dx.doi.org/10.1021/la403864u | Langmuir 2013, 29, 15689–15697

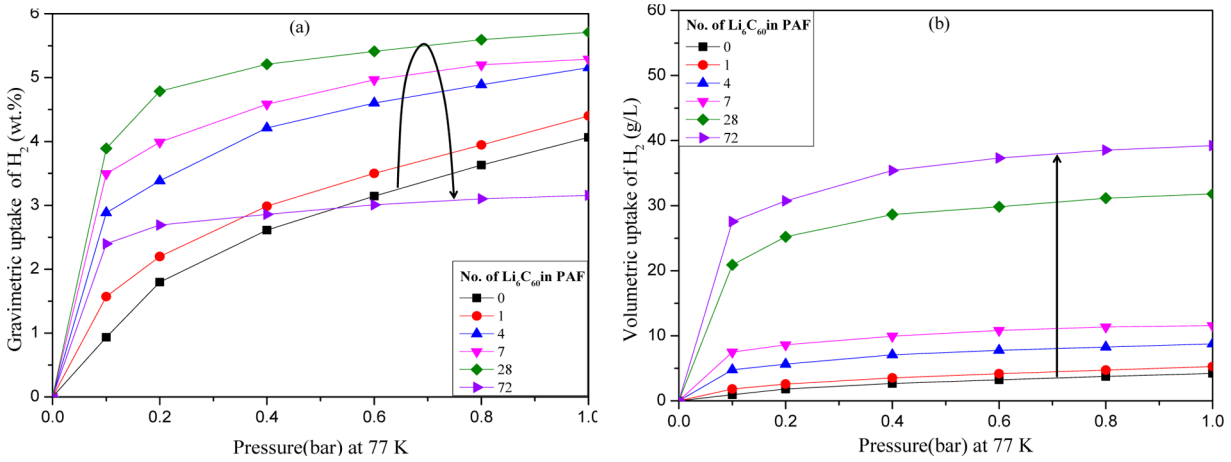

Figure 3. Total H_2 uptake in PAF-304: (a) gravimetric and (b) volumetric uptake embedded with the number of Li_6C_{60} molecules up to 1 bar and 77 K. Arrows indicate increased Li_6C_{60} loading.

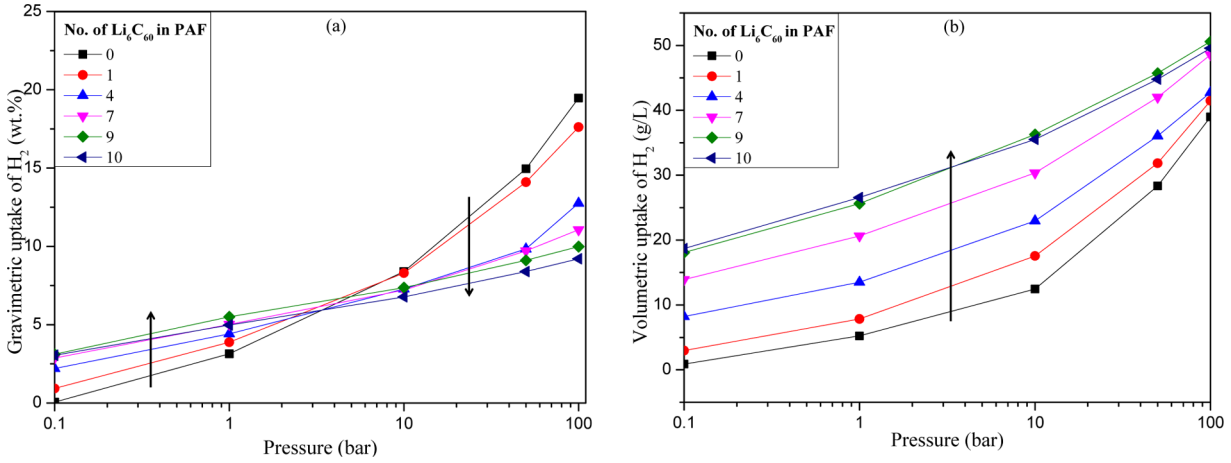

Figure 4. Total H_2 uptake in PAF-303: (a) gravimetric (b) and volumetric uptake embedded with the number of Li_6C_{60} molecules up to 100 bar and 77 K. Arrows indicate increased Li_6C_{60} loading.

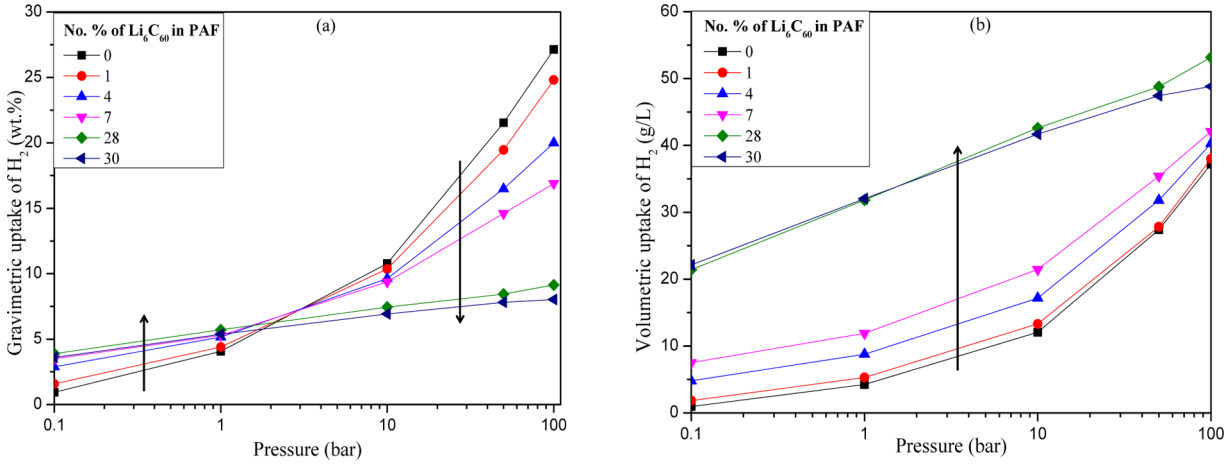

Figure 5. Total H_2 uptake in PAF-304: (a) gravimetric and (b) volumetric embedded with the number of Li_6C_{60} up to 100 bar and 77 K. Arrows indicate increased Li_6C_{60} loading.

Volumetric uptake at high pressures, however, continues to improve with Li_6C_{60} loading, as shown in Figures 4b and 5b. The different trends between gravimetric and volumetric uptake can be explained by the increased material mass with impregnation whereas there is no increase in material volume. Therefore, impregnation is an ideal strategy for enhancing volumetric uptake.

Because excess uptake is also of interest to compare with most experimental results, the predicted volumetric excess and total hydrogen uptake for bare PAFs and impregnated PAFs are

dx.doi.org/10.1021/la403864u | *Langmuir* 2013, 29, 15689−15697

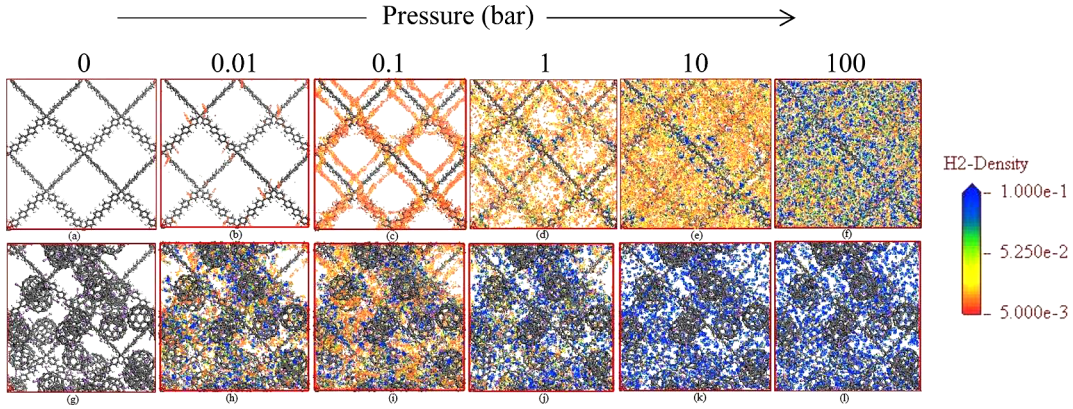

Figure 6. Snapshots of H_2 adsorption in PAF-304 without Li_6C_{60} at 77 K and pressures of (a) 0, (b) 0.01, (c) 0.1, (d) 1, (e) 10, and (f) 100 bar and with $28Li_6C_{60}$ at pressures of (g) 0, (h) 0.01, (i) 0.1, (j) 1, (k) 10, and (l) 100 bar, respectively, with the smallest hydrogen density highlighted in orange and the greatest hydrogen density highlighted in blue.

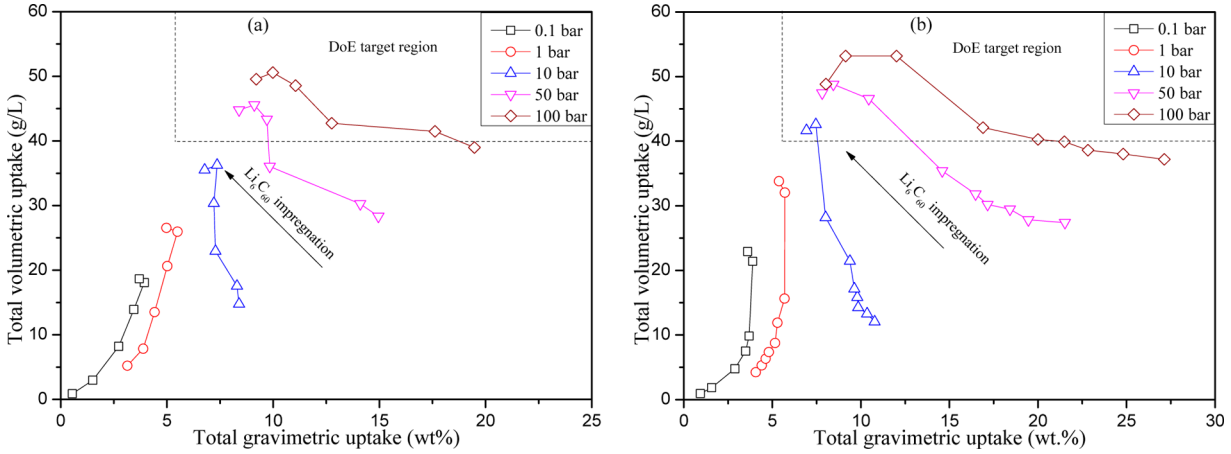

Figure 7. Total volumetric and gravimetric hydrogen uptake with Li_6C_{60} loading in (a) PAF-303 and (b) PAF-304 at 77 K and various pressures.

given in Figure S1 with corresponding structural properties listed in Table S1 of the Supporting Information (SI). A remarkable increase in uptake is observed for both total and excess uptake after impregnation. Excess uptake deviates from total uptake at ambient pressure whereas total uptake continues to increase as the gas-phase density increases.

Snapshots of hydrogen density within the bare framework and the impregnated $28Li_6C_{60}$ framework at various pressures are given in Figure 6. The adsorption at low pressure is mainly on Li_6C_{60} as H_2 is strongly attracted to the lithium ions. The interaction strength between H_2 and Li is 2 orders of magnitude higher than for H_2 to C interactions. A contribution to the strong interaction is the delocalized anionic charge created by Li_6C_{60} described in earlier work by Konstas et al.[37] In addition, Li_6C_{60} has an intrinsic surface area of 6450 $m^2\ g^{-1}$ (Figure S3). Therefore, a combination of greater surface area and stronger adsorption energy leads to a high adsorbed density. As expected, the H_2 density increases with increasing pressure for both materials. The most compelling insight is that the impregnated structure contains a much higher H_2 density than the bare structure. As stated earlier, the total material mass increases significantly with Li_6C_{60} loading while the total material volume remains constant. Therefore, the reason that the total volumetric uptake increases with Li_6C_{60} loading is that the H_2 density increases without an increase in the total material volume.

To understand the effect of Li_6C_{60} impregnation further, Figure 7 displays the calculated H_2 volumetric versus gravimetric uptake with varying pressure and Li_6C_{60} loading. The aim here is to find the right combination of pressure and/or Li_6C_{60} loading to reach both the prescribed DoE target region for gravimetric and volumetric uptake,[11] outlined with dashed lines. In the low-pressure range (0.1−1 bar), both volumetric and gravimetric uptake increase with the impregnation of Li_6C_{60} for PAF-303 and PAF-304. In a medium pressure range (10−50 bar), the volumetric uptake increases but the gravimetric uptake decreases with Li_6C_{60} loading. Finally, at high pressures (~100 bar), there is a concave shape (or seesaw trade-off) with the number of Li_6C_{60} molecules impregnating the PAFs, as observed recently by Goldsmith et al.[48] If volumetric uptake is the top priority for energy storage, then a maximum is obtained by impregnating PAF-303 with $9Li_6C_{60}$'s and PAF-304 with $28Li_6C_{60}$'s. However, if gravimetric and volumetric uptakes are of equal importance, then the optimal Li_6C_{60} loading greatly depends on the required operating conditions. Therefore, it is necessary to define the dependence that uptake has on structural characteristics under certain operating conditions. As presented by Lim et al.,[9] the storage capacity is not the only indicator of performance but rather the working capacity is of critical importance. Figure S4 in the SI illustrates that the empty PAFs without Li_6C_{60} apparently have the largest delivery if cycled between the DoE pressure range of 5−100 bar. However, if cycled between vacuum and 1 bar, the

dx.doi.org/10.1021/la403864u | Langmuir 2013, 29, 15689−15697

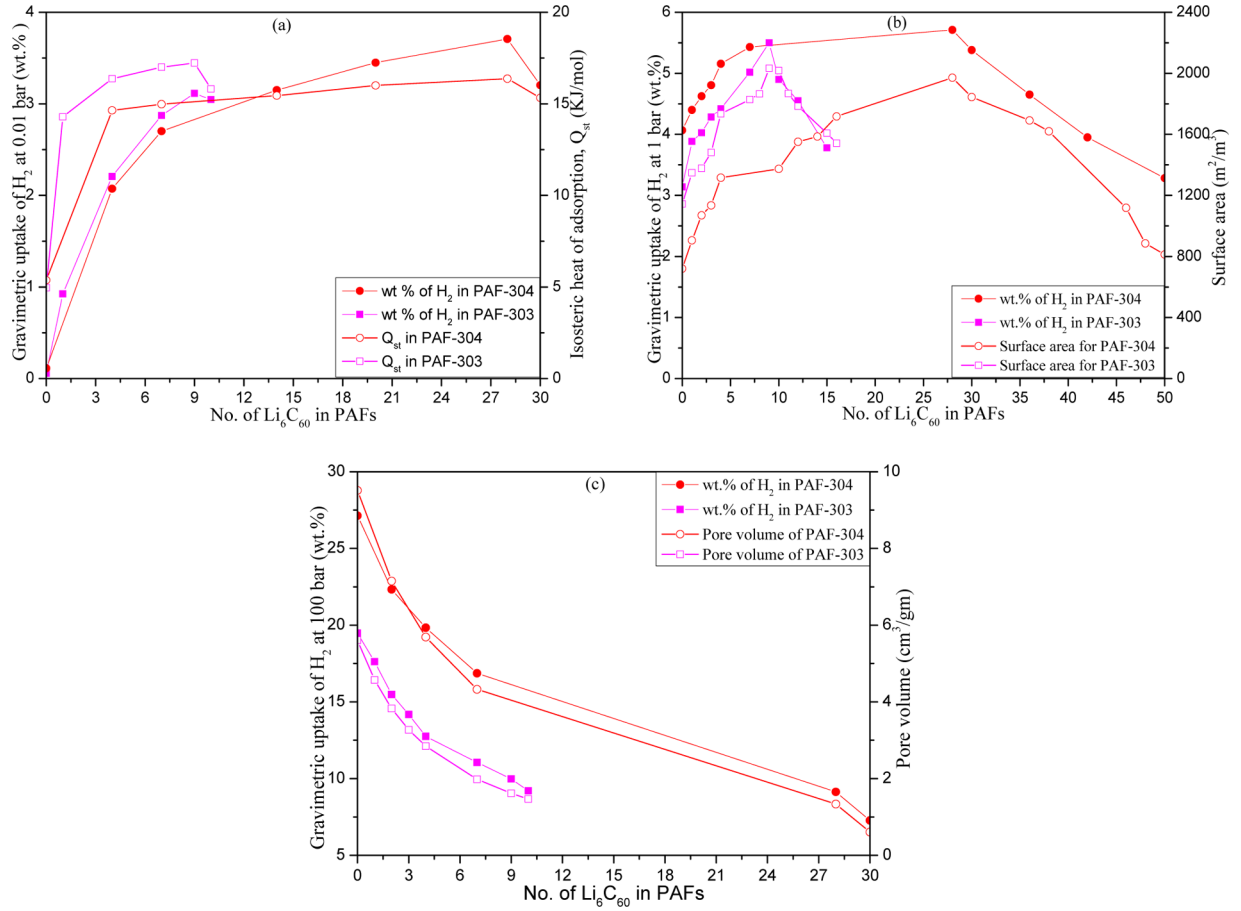

Figure 8. Structure–property relationships among gravimetric H_2 uptake, Li_6C_{60} loading and (a) heat of adsorption at 0.01 bar, (b) surface area at 1 bar, and (c) pore volume at 100 bar.

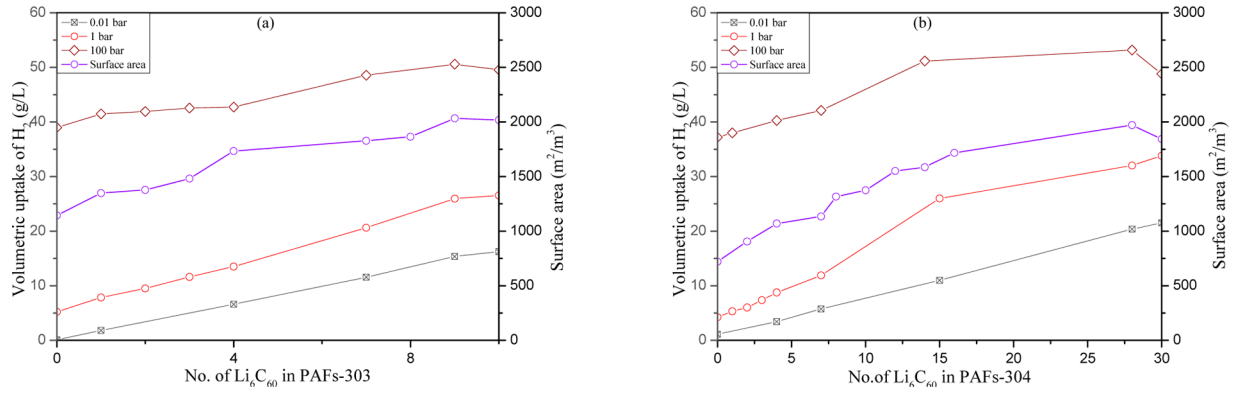

Figure 9. Structure–property relationships among volumetric H_2 uptake, Li_6C_{60} loading, and surface area for (a) PAF-303 and (b) PAF-304.

impregnated PAFs' performance is high with a greater working capacity.

For a closer analysis, gravimetric and volumetric results are presented separately in Figures S5 and S6 of the SI. At 1 bar, the impregnation of $9Li_6C_{60}$ loading within PAF-303 delivered a maximum gravimetric H_2 uptake. In addition, a maximum of 5.71 wt % gravimetric uptake for $28Li_6C_{60}$ loading in PAF-304 has been achieved. Volumetric uptake is also maximized at the same Li_6C_{60} loading for pressures above 10 bar. At 10 bar, the gravimetric uptake is almost constant with an increasing number of Li_6C_{60} molecules, but at 100 bar, the uptake is reduced with Li_6C_{60} loading. The volumetric uptakes showed a more enduring increase with the impregnation of Li_6C_{60} at all pressures compared to the gravimetric uptake. As a result, we can achieve a remarkable enhancement of up to 260% of the volumetric adsorption capacity in PAF-304 at 10 bar, from 12 to 44 g L^{-1} with the impregnation of Li_6C_{60}.

It is noteworthy that if we assume that the hydrogen storage tank is completely filled with the ideal adsorbent then the total uptake may be compared to the DoE targets. However, the cryogenic temperature condition is not within the DoE required operating conditions. In reality, adsorbents are usually compressed into pellets, losing their intrinsic pore volume and creating pellet–pellet gaps. Therefore, the total uptake should at least be accompanied by an estimated loss of pore volume (24% loss according to Dailly and Piorier[49]) to extrapolate to

dx.doi.org/10.1021/la403864u | *Langmuir* 2013, 29, 15689–15697

macroscale system performance. In the case for PAF, the large-scale packing method is yet to be determined, and pore volume loss estimates are unavailable. Nonetheless, with the current predictions one can extrapolate the results to an altered pore volume using the structure−property relationships elucidated further in the article.

In the interest of relating the observed trends in uptake with the structural features such as the heat of adsorption, surface area, and pore volume, Figure 8 for gravimetric uptake and Figure 9 for volumetric uptake are presented. The heat of adsorption is calculated as the pressure-dependent isosteric heat of adsorption; see Figure S8 for the complete data set. As suggested previously, correlations between gravimetric uptake and Li_6C_{60} loading strongly depend on the pressure conditions. For gravimetric uptake, it is clear that the trend in heat of adsorption (at 0.01 bar) with the number of Li_6C_{60} molecules is identical to the trend in gravimetric uptake at 0.01 bar (Figure 8a). Both PAF-303 and PAF-304 have very similar heats of adsorption at low loadings of between 5 and 15 kJ mol^{-1}. According to Mendoza-Corté et al.[50] and Bhatia et al.,[51] the next generation of frameworks targeting hydrogen adsorption with high delivery amounts should be at least as high as 15 kJ mol to reach the DoE gravimetric targets. Therefore, the kinetics of hydrogen adsorption and desorption in PAFs are expected to be more favorable with Li_6C_{60} impregnation.

Furthermore, the surface area correlates with the gravimetric uptake at 1 bar (Figure 8b). Maximum surface areas (m^2/m^3) of 1971 and 2033 are achieved for PAF-304 and PAF-303, respectively, with corresponding numbers of Li_6C_{60} molecules of 28 and 9. Therefore, the maximum H_2 uptake at this pressure is a result of maximizing the surface area. It is clear that the larger the surface area, the greater the gravimetric uptake (in this pressure range).

Pore volume correlates with H_2 uptake at 100 bar (Figure 8c). At 100 bar, as we impregnate more Li_6C_{60}, the pore volume decreases. This decreasing trend is also observed in the case of gravimetric uptake at high pressure,where the hydrogen density is already at a maximum and therefore the available void space is critical. As a result, we obtain excellent correlation at 100 bar.

It is worth noting that these relationships were first observed by Frost et al.[43] by varying the ligand length of MOFs. Frost et al. also observed the effect of the heat of adsorption, surface area, and pore volume at different pressures. Here we have confirmed these trends with impregnation that can be understood as an inverse action with respect to the ligand extension of Frost et al., where Frost et al. increased the pore volume with modification whereas we decrease the pore volume with modification. In addition to these structural parameters, the pore size distribution (calculated using Zeo++[52]) shows that the large pores are gradually filled with lithiated fullerenes, creating smaller pores and wider size distributions (Figure S2). For example, an empty PAF-303 pore of 21 Å becomes filled after impregnation, creating smaller pores ranging from 6 to 16 Å. This also explains the high heat of adsorption with loading and the high uptake and low pressures. More details are found in the Supporting Information.

Interestingly, for volumetric uptake as shown in Figure 9, the surface area correlates with uptake at all pressures (ranging from 0.01 to 100 bar). As a general trend, the volumetric uptake is enhanced with increased volumetric surface area for all pressures. By impregnating the PAF with lithiated fullerenes, the available surface area for hydrogen adsorption is increased. Because the hydrogen density on the surface is much greater than in the gas phase, there is a continual benefit from incorporating lithiated fullerenes.

Finally, we calculated the volumetric uptake of H_2 in bare PAF-304 and impregnated $28Li_6C_{60}$@PAF-304 at varying temperature from 50 to 300 K (Figure S7 in the SI). Above the critical temperature (33 K), the H_2 density increased rapidly with pressure. In the cryogenic temperature range (50−150 K), the volumetric uptake increases with the impregnation of Li_6C_{60}. At high pressure and high temperature (243 K), we found the highest uptake of 23.5 g L^{-1} for $28Li_6C_{60}$@PAF-304 whereas for bare PAF the value is 9.56 g L^{-1}. These results demonstrate the benefit of impregnation across all pressures and temperatures. Results such as these are critical for material and process optimization for industrial-scale applications.

IV. CONCLUSIONS

The adsorption of hydrogen within Li_6C_{60} impregnated PAF materials have been investigated via GCMC simulation, with the goal of reaching the DoE capacity targets for on-board hydrogen storage at cryogenic temperature (not within DoE specifications). Despite an apparent loss of free volume related to pore filling by lithiated fullerenes, the adsorption capacity was increased at low pressures for gravimetric uptake and increased at all pressures for volumetric uptake. This improvement strategy may remove the need for high-pressure vessels. The incorporation of Li_6C_{60} into PAF-303 and PAF-304 exceeds the 2017 DoE gravimetric target at a low 1 bar and reaches the 2017 DoE volumetric target at a pressure range of 10−20 bar at cryogenic conditions. Although the capacity targets seem to be achievable, the operating conditions are outside of the DoE prescriptions. The idea of incorporating Li_6C_{60} inside PAF-303 and PAF-304 opens a new avenue for the design, composition, and fabrication of highly porous materials with an exceptional capacity for hydrogen storage and other applications.

■ ASSOCIATED CONTENT

Supporting Information

Comparison between total and excess uptake, table of structural characteristics, simulated uptake under other operating conditions (50−300 K and 0−100 bar), pore size distribution, surface area of Li_6C_{60}, and comparison between Q_{st} and pressure. This material is available free of charge via the Internet at http://pubs.acs.org/.

■ AUTHOR INFORMATION

Corresponding Author

*E-mail: aaron.thornton@csiro.au.

Notes

The authors declare no competing financial interest.

■ ACKNOWLEDGMENTS

A.A. acknowledges the top-up scholarship provided by the CSIRO Computational and Simulation Sciences Transformational Capability Platform and the full scholarship provided by Swinburne University. We acknowledge the computational facilities and services provided through the CSIRO Advanced Scientific Computing. R.B. acknowledges funding from the Scientific and Industry Endowment Fund through the Solving the Energy Waste Roadblock project.

REFERENCES

(1) Sumida, K.; Hill, M. R.; Horike, S.; Dailly, A.; Long, J. R. Synthesis and Hydrogen Storage Properties of $Be_{12}(OH)_{12}$(1,3,5-benzenetribenzoate)$_4$. *J. Am. Chem. Soc.* **2009**, *131*, 15120−15121.

(2) Han, S. S.; Goddard, W. A. Lithium-Doped Metal-Organic Frameworks for Reversible H_2 Storage at Ambient Temperature. *J. Am. Chem. Soc.* **2007**, *129*, 8422−8423.

(3) Belof, J. L.; Stern, A. C.; Space, B. A Predictive Model of Hydrogen Sorption for Metal−Organic Materials. *J. Phys. Chem. C* **2009**, *113*, 9316−9320.

(4) Kaye, S. S.; Dailly, A.; Yaghi, O. M.; Long, J. R. Impact of Preparation and Handling on the Hydrogen Storage Properties of Zn_4O(1, 4-benzenedicarboxylate)$_3$ (MOF-5). *J. Am. Chem. Soc.* **2007**, *129*, 14176−14177.

(5) Cao, D.; Lan, J.; Wang, W.; Smit, B. Lithium-Doped 3D Covalent Organic Frameworks: High-Capacity Hydrogen Storage Materials. *Angew. Chem., Int. Ed.* **2009**, *121*, 4824−4827.

(6) Lan, J.; Cao, D.; Wang, W.; Smit, B. Doping of Alkali, Alkaline-Earth, and Transition Metals in Covalent-Organic Frameworks for Enhancing CO_2 Capture by First-Principles Calculations and Molecular Simulations. *ACS Nano* **2010**, *4*, 4225−4237.

(7) Furukawa, S.-i.; Nitta, T. Non-Equilibrium Molecular Dynamics Simulation Studies on Gas Permeation across Carbon Membranes with Different Pore Shape Composed of Micro-Graphite Crystallites. *J. Membr. Sci.* **2000**, *178*, 107−119.

(8) Zhong, Z.; Xiong, Z.; Sun, L.; Luo, J.; Chen, P.; Wu, X.; Lin, J.; Tan, K. Nanosized Nickel (or Cobalt)/Graphite Composites for Hydrogen Storage. *J. Phys. Chem. B* **2002**, *106*, 9507−9513.

(9) Lim, W.-X.; Thornton, A. W.; Hill, A. J.; Cox, B. J.; Hill, J. M.; Hill, M. R. High Performance Hydrogen Storage from Be-BTB Metal−Organic Framework at Room Temperature. *Langmuir* **2013**, *29*, 8524−8533.

(10) Frost, H.; Düren, T.; Snurr, R. Q. Effects of Surface Area, Free Volume, and Heat of Adsorption on Hydrogen Uptake in Metal-Organic Frameworks. *J. Phys. Chem. B* **2006**, *110*, 9565−9570.

(11) Hydrogen Storage Summary of Annual Merit Review of the Hydrogen Storage Sub-Program. U.S. Department of Energy http://www.hydrogen.energy.gov/pdfs/review12/55568-04_storage.pdf, 2012.

(12) Chakraborty, A.; Kumar, S. Thermal Management and Desorption Modeling of a Cryo-Adsorbent Hydrogen Storage System. *Int. J. Hydrogen Energy* **2013**, *39*, 3973−3986.

(13) Kumar, V. S.; Kumar, S. Generalized Model Development for a Cryo-Adsorber and 1-D Results for the Isobaric Refueling Period. *Int. J. Hydrogen Energy* **2010**, *35*, 3598−3609.

(14) Senthil Kumar, V. A Generalized Cryo-Adsorber Model and 2-D Refueling Results. *Int. J. Hydrogen Energy* **2011**, *36*, 15239−15249.

(15) Poirier, E.; Dailly, A. Thermodynamic Study of the Adsorbed Hydrogen Phase in Cu-Based Metal-Organic Frameworks at Cryogenic Temperatures. *Energy Environ. Sci.* **2009**, *2*, 420−425.

(16) Raymond, A. W.; Reiter, J. *Modeling and Testing of Cryo-Adsorbent Hydrogen Storage Tanks with Improved Thermal Isolation*; AIP Conference Proceedings, 2012; p 765.

(17) Kopyscinski, J.; Schildhauer, T. J.; Biollaz, S. Production of Synthetic Natural Gas (SNG) from Coal and Dry Biomass−A Technology Review from 1950 to 2009. *Fuel* **2010**, *89*, 1763−1783.

(18) Wang, J.; Wan, W. Factors Influencing Fermentative Hydrogen Production: A Review. *Int. J. Hydrogen Energy* **2009**, *34* (), 799−811.

(19) Das, D.; Veziroglu, T. N. Advances in Biological Hydrogen Production Processes. *Int. J. Hydrogen Energy* **2008**, *33*, 6046−6057.

(20) Yu, J.; Qi, L.; Jaroniec, M. Hydrogen Production by Photocatalytic Water Splitting over Pt/TiO_2 Nanosheets with Exposed (001) Facets. *J. Phys. Chem. C* **2010**, *114*, 13118−13125.

(21) Rowsell, J. L.; Yaghi, O. M. Strategies for Hydrogen Storage in Metal−Organic Frameworks. *Angew. Chem., Int. Ed.* **2005**, *44*, 4670−4679.

(22) Akutsu, H.; Nagamori, T. Conformational Analysis of the Polar Head Group in Phosphatidylcholine Bilayers: A Structural Change Induced by Cations. *Biochemistry* **1991**, *30*, 4510−4516.

(23) Ma, S.; Zhou, H.-C. Gas Storage in Porous Metal−Organic Frameworks for Clean Energy Applications. *Chem. Commun.* **2010**, *46*, 44−53.

(24) Collins, D. J.; Zhou, H.-C. Hydrogen Storage in Metal-Organic Frameworks. *J. Mater. Chem.* **2007**, *17*, 3154−3160.

(25) Isaeva, V. I.; Kustov, L. M. Metal-Organic Frameworks—New Materials for Hydrogen Storage. *Russ. J. Gen. Chem.* **2007**, *77*, 721−739.

(26) Lin, X.; Jia, J.; Hubberstey, P.; Schroder, M.; Champness, N. R. Hydrogen Storage in Metal-Organic Frameworks. *CrystEngComm* **2007**, *9*, 438−448.

(27) Yuan, D.; Zhao, D.; Sun, D.; Zhou, H.-C. An Isoreticular Series of Metal−Organic Frameworks with Dendritic Hexacarboxylate Ligands and Exceptionally High Gas-Uptake Capacity. *Angew. Chem., Int. Ed.* **2010**, *49*, 5357−5361.

(28) El-Kaderi, H. M.; Hunt, J. R.; Mendoza-Cortés, J. L.; Côté, A. P.; Taylor, R. E.; O'Keeffe, M.; Yaghi, O. M. Designed Synthesis of 3D Covalent Organic Frameworks. *Science* **2007**, *316*, 268−272.

(29) Hunt, J. R.; Doonan, C. J.; LeVangie, J. D.; Côté, A. P.; Yaghi, O. M. Reticular Synthesis of Covalent Organic Borosilicate Frameworks. *J. Am. Chem. Soc.* **2008**, *130*, 11872−11873.

(30) Côté, A. P.; Benin, A. I.; Ockwig, N. W.; O'Keeffe, M.; Matzger, A. J.; Yaghi, O. M. Porous, Crystalline, Covalent Organic Frameworks. *Science* **2005**, *310*, 1166−1170.

(31) Côté, A. P.; El-Kaderi, H. M.; Furukawa, H.; Hunt, J. R.; Yaghi, O. M. Reticular Synthesis of Microporous and Mesoporous 2D Covalent Organic Frameworks. *J. Am. Chem. Soc.* **2007**, *129*, 12914−12915.

(32) Mendoza-Cortes, J. L.; Goddard, W. A., III; Furukawa, H.; Yaghi, O. M. A Covalent Organic Framework that Exceeds the DOE 2015 Volumetric Target for H_2 Uptake at 298 K. *J. Phys. Chem. Lett.* **2012**, *3*, 2671−2675.

(33) Farha, O. K.; Eryazici, I.; Jeong, N. C.; Hauser, B. G.; Wilmer, C. E.; Sarjeant, A. A.; Snurr, R. Q.; Nguyen, S. T.; Yazaydin, A. Ö.; Hupp, J. T. Metal−Organic Framework Materials with Ultrahigh Surface Areas: Is the Sky the Limit? *J. Am. Chem. Soc.* **2012**, *134*, 15016−15021.

(34) Babarao, R.; Jiang, J. Exceptionally High CO_2 Storage in Covalent-Organic Frameworks: Atomistic Simulation Study. *Energy Environ. Sci.* **2008**, *1*, 139−143.

(35) Ben, T.; Ren, H.; Ma, S.; Cao, D.; Lan, J.; Jing, X.; Wang, W.; Xu, J.; Deng, F.; Simmons, J. M.; Qiu, S.; Zhu, G. Targeted Synthesis of a Porous Aromatic Framework with High Stability and Exceptionally High Surface Area. *Angew. Chem., Int. Ed.* **2009**, *48*, 9457−9460.

(36) Yuan, D.; Lu, W.; Zhao, D.; Zhou, H. C. Highly Stable Porous Polymer Networks with Exceptionally High Gas-Uptake Capacities. *Adv. Mater.* **2011**, *23*, 3723−3725.

(37) Konstas, K.; Taylor, J. W.; Thornton, A. W.; Doherty, C. M.; Lim, W. X.; Bastow, T. J.; Kennedy, D. F.; Wood, C. D.; Cox, B. J.; Hill, J. M. Lithiated Porous Aromatic Frameworks with Exceptional Gas Storage Capacity. *Angew. Chem., Int. Ed. Engl.* **2012**, *51*, 6639−6642.

(38) Suh, M. P.; Park, H. J.; Prasad, T. K.; Lim, D.-W. Hydrogen Storage in Metal−Organic Frameworks. *Chem. Rev.* **2011**, *112*, 782−835.

(39) Murray, L. J.; Dincă, M.; Long, J. R. Hydrogen Storage in Metal−Organic Frameworks. *Chem. Soc. Rev.* **2009**, *38*, 1294−1314.

(40) Thornton, A. W.; Nairn, K. M.; Hill, J. M.; Hill, A. J.; Hill, M. R. Metal− Organic Frameworks Impregnated with Magnesium-Decorated Fullerenes for Methane and Hydrogen Storage. *J. Am. Chem. Soc.* **2009**, *131*, 10662−10669.

(41) Lan, J.; Cao, D.; Wang, W.; Ben, T.; Zhu, G. High-Capacity Hydrogen Storage in Porous Aromatic Frameworks with Diamond-like Structure. *J. Phys. Chem. Lett.* **2010**, *1* (), 978−981.

(42) Rao, D.; Lu, R.; Xiao, C.; Kan, E.; Deng, K. Lithium-Doped MOF Impregnated with Lithium-Coated Fullerenes: A Hydrogen Storage Route for High Gravimetric and Volumetric Uptakes at Ambient Temperatures. *Chem. Commun.* **2011**, *47*, 7698−7700.

(43) Frost, H.; Duren, T.; Snurr, R. Q. Effects of Surface Area, Free Volume, And Heat of Adsorption on Hydrogen Uptake in Metal-Organic Frameworks. *J. Phys. Chem. B* **2006**, *110*, 9565−9570.
(44) Hill, A. J.; Jones, P. L.; Lind, J. H.; Pearsall, G. W. A Positron Annihilation Lifetime Study of Isothermal Structural Relaxation in Bisphenol-A Polycarbonate. *J. Polym. Sci., Part A: Polym. Chem.* **1988**, *26*, 1541−1552.
(45) Sun, Q.; Jena, P.; Wang, Q.; Marquez, M. First-Principles Study of Hydrogen Storage on $Li_{12}C_{60}$. *J. Am. Chem. Soc.* **2006**, *128*, 9741−9745.
(46) Teprovich, J. A.; Wellons, M. S.; Lascola, R.; Hwang, S.-J.; Ward, P. A.; Compton, R. N.; Zidan, R. Synthesis and Characterization of a Lithium-Doped Fullerane (Li_x-C_{60}-H_y) for Reversible Hydrogen Storage. *Nano Lett.* **2011**, *12*, 582−589.
(47) Meng, Z.; Lu, R.; Rao, D.; Kan, E.; Xiao, C.; Deng, K. Catenated Metal-Organic Frameworks: Promising Hydrogen Purification Materials and High Hydrogen Storage Medium with Further Lithium Doping. *Int. J. Hydrogen Energy* **2013**, *38*, 9811−9818.
(48) Goldsmith, J.; Wong-Foy, A. G.; Cafarella, M. J.; Siegel, D. J. Theoretical Limits of Hydrogen Storage in Metal−Organic Frameworks: Opportunities and Trade-Offs. *Chem. Mater.* **2013**, *25*, 3373−3382.
(49) Dailly, A.; Poirier, E. Evaluation of an Industrial Pilot Scale Densified MOF-177 Adsorbent as an on-Board Hydrogen Storage Medium. *Energy Environ. Sci.* **2011**, *4*, 3527−3534.
(50) Mendoza-Cortés, J. L.; Han, S. S.; Goddard, W. A., III. High H_2 Uptake in Li-, Na-, K-Metalated Covalent Organic Frameworks and Metal Organic Frameworks at 298 K. *J. Phys. Chem. A* **2012**, *116*, 1621−1631.
(51) Bhatia, S. K.; Myers, A. L. Optimum Conditions for Adsorptive Storage. *Langmuir* **2006**, *22* (), 1688−1700.
(52) Willems, T. F.; Rycroft, C. H.; Kazi, M.; Meza, J. C.; Haranczyk, M. Algorithms and Tools for High-Throughput Geometry-Based Analysis of Crystalline Porous Materials. *Microporous Mesoporous Mater.* **2012**, *149*, 134−141.